

**DESIGN AND ANALYSIS OF THIN WALLED SEMI-MONOCOQUE WING  
STRUCTURES USING DIFFERENT STRUCTURAL IDEALIZATIONS IN  
THE PRELIMINARY DESIGN PHASE**

Odeh Dababneh<sup>1</sup>  
Department of Aerospace Eng., Middle East  
Technical University  
Ankara, Turkey

Altan Kayran<sup>2</sup>  
Department of Aerospace Eng., Middle East  
Technical University  
Ankara, Turkey

**ABSTRACT**

In modeling an aircraft wing, structural idealizations are often employed in hand calculations to simplify the structural analysis. In real applications of structural design and analysis, finite element methods are used because of the complexity of the geometry, combined and complex loading conditions. This article gives a comprehensive study on the effect of using different structural idealizations on the design and analysis of thin walled semi-monocoque wing structures in the preliminary design phase. In the design part of the article, wing structures are designed using two different structural idealizations that are typically used in the preliminary design phase. In the structural analysis part, finite element analysis of one of the designed wing configurations is performed using six different one and two dimensional element pairs which are typically used to model the sub-elements of semi-monocoque wing structures. The effect of using different finite element types on the analysis results of the wing structure, which is designed by the simplified method using two different idealization approaches, is investigated. Comparisons are also made between the analysis results of the finite element solution and the simplified method, and the applicability of the simplified method in the preliminary design phase is investigated for the wing configuration studied in the article. During the analysis study, depending on the mesh size used, conclusions are also inferred with regard to the deficiency of certain element types in handling the true external load acting on the wing structure.

**KEYWORDS:** Structural Design, Structural Idealization, Wing Torque Box, Finite element Analysis

**INTRODUCTION**

In the early development and manufacturing of flight vehicles, the major focus of structural design was strength. Nowadays, the use of lighter structures in aerospace structural design is becoming an important issue. Aerospace structures mainly consist of reinforced thin walled straight and curved members except in regions where high local loads have to be resisted such as hard points or main frames. Most of the thin walled structural members of aerospace vehicles have multi-cell box beam configurations made of semi-monocoque construction. By reinforcing thin walled shells with stiffeners, it is possible to prevent various failure modes and structural stability problems, and lighter structures can be manufactured.

<sup>1</sup> Grad. Student, e132180@metu.edu.tr

<sup>2</sup> Prof. Dr., akayran@metu.edu.tr

Lifting surfaces such as wing, tail plane, control surfaces and aircraft fuselage are some examples of thin walled sub-structures reinforced by stiffeners. In modeling reinforced thin walled aerospace sub-structures, structural idealizations are often employed in simplified methods. Structural idealizations utilized in simplified methods include certain assumptions with regard to the load carrying capability of thin walled shell structures such as wing skins, ribs, spar webs and reinforcing members such as spar caps, stringers etc. Typical structural idealizations that are used in the simplified structural analysis of reinforced thin walled shell structures are based on the assumption that thin walled shell members mainly carry either shear loads only or shear plus axial loads, whereas reinforcements mainly carry axial loads. These idealizations are widely used in standard textbooks of aerospace structural design and analysis [4-6, 8, 10-12]. With the simplified method of analysis, structural analysis problems of aerospace structures, which are complex and can not be solved by analytical methods, can be solved by hand calculations, and an initial sizing can be obtained in the preliminary design phase. In the aerospace structures education, simplified method of analysis is a very powerful tool which eases the explanation of concepts. However, in real applications because of the complexity of the geometry and loading conditions of aerospace sub-structures, finite element methods are often used in almost all phases of the structural design and analysis. The use of finite element method necessitates the appropriate choice of element types in modeling the true behavior of a structural component. The correct use of finite element analysis is very critical in ascertaining the true failure mode of the structural member. A very interesting work on the correct use of finite element models for stress analysis of aircraft is given by Vaughan and Daniel [5]. In this study, authors presented examples on the correct and incorrect structural analysis by means of finite element method.

### WING GEOMETRY AND STRUCTURAL LAYOUT

The basic wing design is assumed to be for a single utility aircraft having a maximum take-off weight of 1460 kg and minimum operating weight of 861 kg. The wing structure is straight and unswept, and wing has a NACA 2412 airfoil profile with a rectangular planform, with a chord length of 1.524 m and semi-span of 4.572 m. Wing design is done for a two-spar, two-stiffener and seven-rib configuration dividing the wing into 6 equal sections of length 0.762 m. The root extensions of the front and rear spars are of 0.5 m in length. Figure 1 shows the structural lay-out of the wing structure.

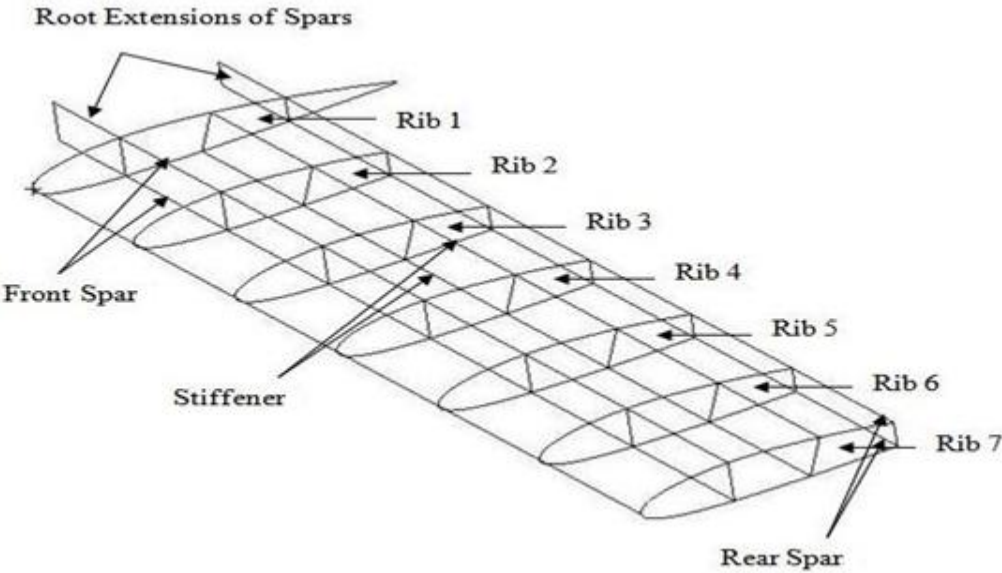


Figure 1. Final wing geometry and structural layout

## External Aerodynamic and Internal Loads

In the simplified method of analysis, the external aerodynamic load is calculated as a line lift and pitching moment acting span-wise at the 25 % chord length. The span-wise distribution of the lift and the pitching moment are calculated by ESDU 95010 [9], and the limit loads are calculated at the corner points of the V-N diagram established in accordance with appendix A of FAR 23 [3]. Internal loads are then calculated as sectional bending moment, pitching moment and shear force acting at the 25 % chord-line. Figures 2 and 3 show spanwise lift and pitching moment distributions at the 25 % of the chord measured from the leading edge for the minimum maneuvering speed  $V_A$  of 145 Knots and at the maximum positive load factor of 4.4. These conditions correspond to the upper left corner of the V-N diagram – point A for the particular airplane.

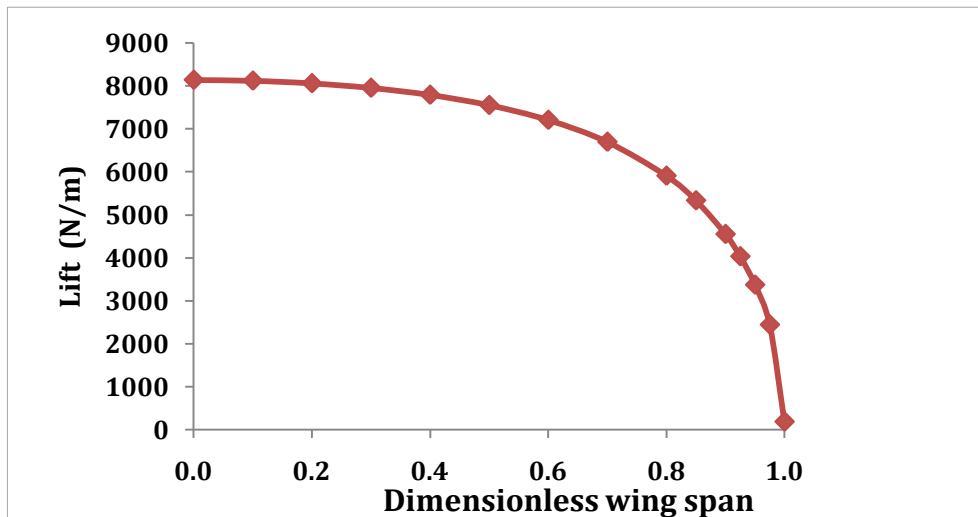


Figure 2. Span-wise variation of aerodynamic lift distribution

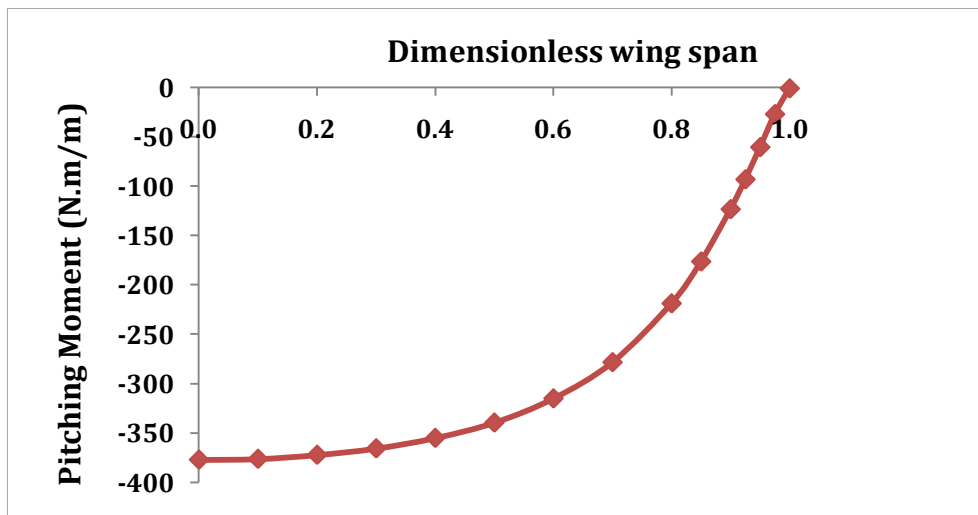


Figure 3. Span-wise variation of aerodynamic pitching moment distribution

Figures 4-6 show the sectional shear force, sectional bending moment and the sectional pitching moment curves which are calculated based on the external loading given in Figs. 2 and 3. Sectional internal forces are calculated by the method described by Bruhn [11] in a discrete fashion, but in Figs.4-6, continuous curves are drawn with respect to the dimensionless span.

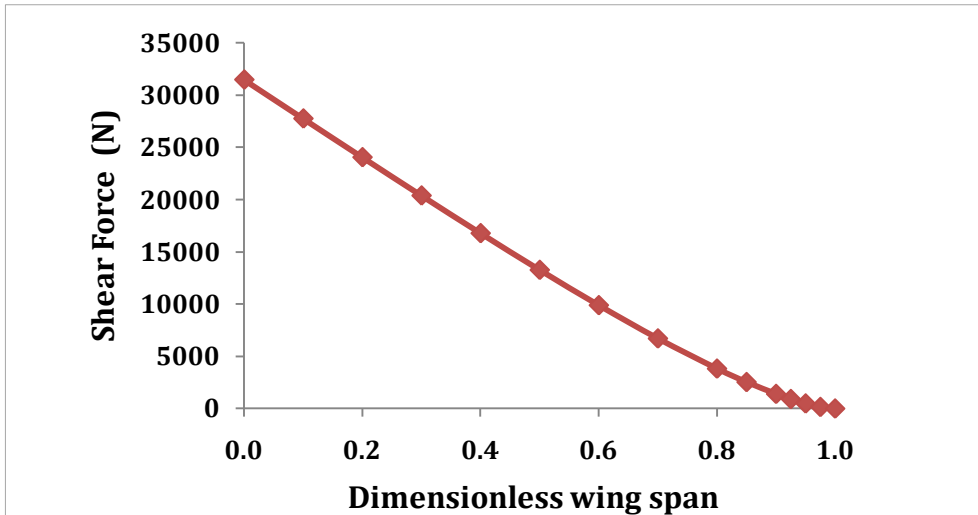


Figure 4. Span-wise sectional shear force distribution

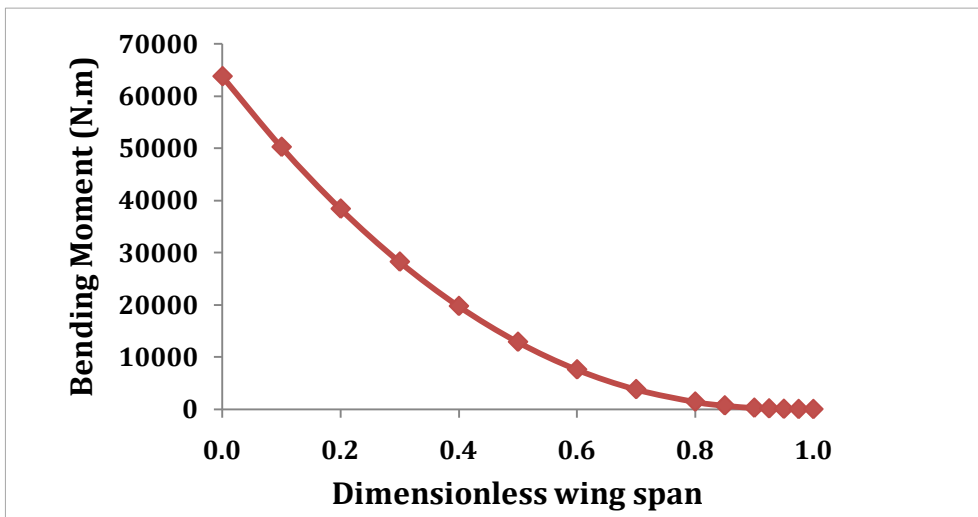


Figure 5. Span-wise sectional bending moment distribution

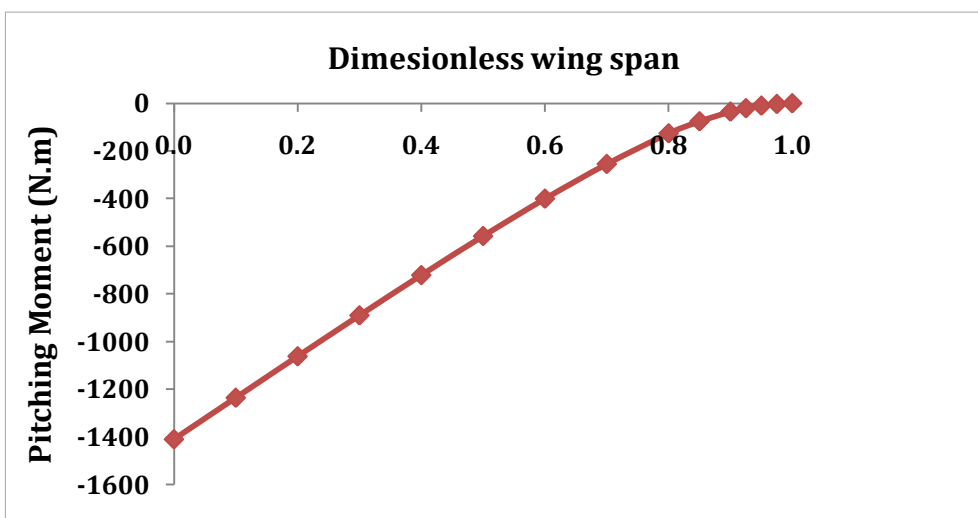


Figure 6. Span-wise sectional pitching moment distribution

## Description of the Design and Analysis Methodology

### Design of semi-monocoque wing structures by the simplified method of analysis

In the first part of the article, a preliminary wing design is performed using two different structural idealizations by the simplified method based analysis. The main goal of the design part of the article is not only to give concise information on the design procedure using structural idealizations that are typically employed in the design phase, but also to come up with a reasonably sized wing structure which will be used in the analysis and optimization phases, and make comparative study of the finite element based analysis and optimization studies with the analysis and iteration based optimization study conducted by the simplified method. It should be noted that optimization part is treated in a separate article, therefore description and results of the structural optimization of the wing configuration are not given in the present article. In the simplified method, the wing is treated as a beam having axial, bending and torsional stiffness. In the first idealization, thin walled shell members are assumed to carry shear load and spar flanges and stringers are assumed to carry axial load only due to bending and/or pure axial load. In the second idealization, thin walled shell members are assumed to carry shear and axial load, due to bending and/or pure axial load, and spar flanges and stringers are again assumed to carry axial load only due to bending and/or pure axial load. In both idealizations, it assumed that free warping prevails away from the restraint end, and torsion induces no axial stress in the one dimensional and two dimensional structural members of the wing. Figure 7 gives the line sketch of the wing section which shows the spar and stringer locations and skin and web thicknesses which are taken as the design variables. In the design process, front spar location is allowed to vary between %20 - %25 of the chord length, rear spar location is allowed to vary between %65 - %75 of the chord length, and stringers are allowed to vary between %30 - %50 of the chord length.

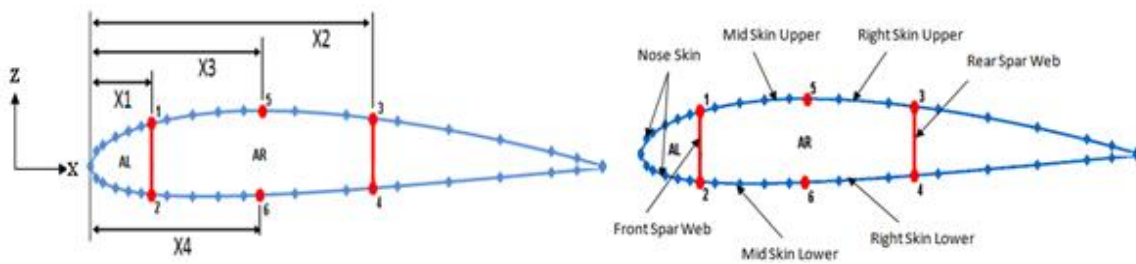


Figure 7. Spar and stringer locations and skin and web thickness definitions

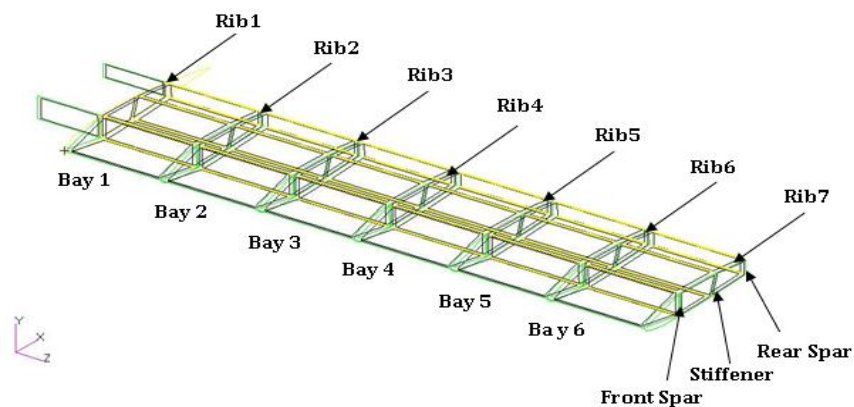


Figure 8. Rib locations along the span of the wing

To simplify the overall model, the trailing edge part behind the rear spar is not considered in the design process. In addition, only a single stringer is considered on the upper and lower skin between the front and the rear spar, and rib positions are taken at constant intervals, along the span of the wing, as shown in Fig. 8. In the design process, sheet thicknesses and spar flange and stringer areas

are kept constant in each bay and they are allowed to change discretely at the rib stations. Design of the wing structure is performed based on the following criteria for the structural idealizations employed in the study.

Design criteria for structural idealization 1 (skins and webs carry shear load only and spar flanges and stringers carry axial stress)

- Maximum shear stresses in the skins and webs of each bay should be less than the shear stress allowable
- Maximum axial stress in the spar flange and stringers should be less than the stress allowable
- Local shear buckling of the wing skins and spar webs should be prevented in each bay

Design criteria for structural idealization 2 (skins and webs carry shear and axial load and spar flanges and stringers carry axial stress)

- Maximum Von-Misses stresses in the skins and webs of each bay should be less than the stress allowable
- Maximum axial stress in the spar flange and stringers should be less than the stress allowable
- Combined tension and shear local buckling of the lower wing skins should be prevented
- Combined compression and shear local buckling of the upper wing skins should be prevented
- Combined bending and shear local buckling of the spar webs should be prevented

In the first idealization, since the inertia of the skins and webs are not considered, shear flows are constant on the wing skins and webs between the spar flange and stringers which are regarded as point areas, as shown in Fig. 7. In the second idealization, inertia of the wing skins and spar webs are also taken into consideration, thus shear flow varies along the wing skins and spar webs. Therefore, in the second idealization, discrete monitor points are defined to calculate the shear flows. The monitor points for shear flow calculations are selected right before and right after each flange and stringer, as shown in Fig.9.

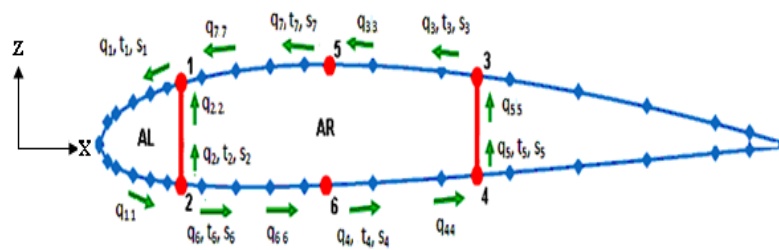


**Figure 9. Shear Flow definitions used in the second structural idealization**

During the design process, for strength checks, stresses are calculated at the inboard edge of each bay, whereas for local buckling checks, average stresses are calculated on the skin and spar web panels for each bay. In both structural idealizations, since cambered airfoils do not have a plane of symmetry, axial stresses are calculated by the unsymmetric beam bending theory. During the design process both continuous and discrete choice of sheet thicknesses and flange/stringer areas are used. In the continuous approach, two separate factors are selected to increment the sheet thicknesses and flange/stringer areas until all stress and buckling constraints are satisfied in each bay. In the discrete approach, standard sheet thicknesses and flange/stringer areas are used in the iterative solution, and selections are made from lists for the standard sheet thickness and flange/stringer area [1, 7, 11]. A Matlab code is written which iterates over the spar and flange locations shown in Fig.7, and over the thickness and flange areas until minimum weight configurations are obtained for each choice of spar and flange/stringer locations.

The initial iterations showed that for both idealizations best locations for the spar and stringer locations are at %25 chord length for the front spar, %70 chord length for the rear spar, %50 chord length for the upper stringer and %46 chord length for the lower stringer. These values do not give absolute minimum weights for each idealization, but they are considered to be the best ones when both structural idealizations are considered. For the spar and stringer locations chosen, minimum weight

designs are performed for the external aerodynamic loading calculated at the minimum maneuvering speed and dive speed both at maximum positive load factor. The results are summarized in Table 1, for both structural idealizations employed during the design process. Table 1 shows that wing designs, which are based on the external loading calculated at the dive speed and positive maximum angle of attack, are slightly heavier than the wing designs based on the aerodynamic load calculated at minimum maneuvering speed and maximum positive load factor. Although the sectional bending moments and shear forces are nearly same for the minimum maneuvering speed and dive speed flight conditions, sectional pitching moments calculated for the dive speed flight condition is higher than the minimum maneuvering speed flight condition. Therefore, the main reason for the higher weight obtained for the dive speed flight condition is higher sectional pitching moment that is calculated at the dive speed condition. Table 1 also shows that use of second structural idealization results in approximately 10 kg lighter mass in the final configuration which is determined in an iterative fashion without employing optimization methods.

**Table 1. Minimum wing masses obtained for both idealizations**

External load	Minimum maneuvering speed at maximum positive load factor	Dive speed at maximum positive load factor
<b>Method</b>	<b>Structural idealization 1</b>	
<i>Continuous</i>	62.9 kg	64.2 kg
<i>Discrete</i>	67.7 kg	69.6 kg
<b>Method</b>	<b>Structural idealization 2</b>	
<i>Continuous</i>	52.2 kg	52.5 kg
<i>Discrete</i>	57.6 kg	58.3 kg

Figure 10 shows the mass breakdown of the wing configurations designed by employing both structural idealizations for the minimum maneuvering speed flight condition. From Fig. 11, it can be seen that since in the second idealization, wing skins and spar webs are also allowed to carry axial load, total skin and spar web masses obtained by using the second idealization are higher than the corresponding masses of the first idealization. On the other hand, since in the first idealization, spar flanges and stringers are assumed to carry all the axial load, the total flange and stringer mass obtained by using the first idealization is considerably higher than the total flange and stringer mass obtained by the second idealization. Therefore, it can be concluded that the mass of the spar flanges and the stringers account for the higher mass of the final configuration of the wing structure, which is designed using the first structural idealization.

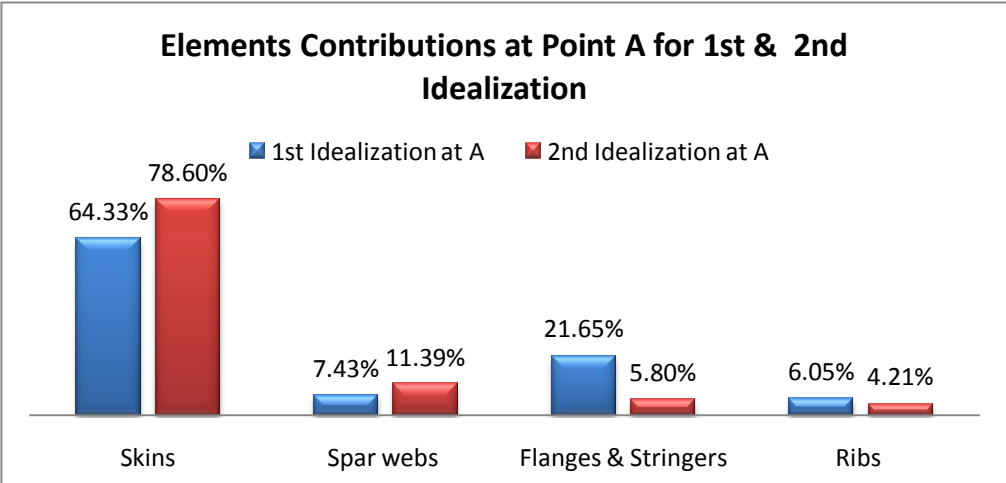


**Figure 10. Mass breakdown of the wing configurations designed using structural idealizations 1 and 2**

It should be noted that in the second idealization, skin and spar web thicknesses obtained after satisfying the stress and local buckling constraints provide sufficient overall inertia such that small spar flange and stringer areas turn out to satisfy the axial stress constraints for these one dimensional members. Therefore, total mass of the spar flanges and the stringers are considerably small

compared to the total flange and stringer mass obtained by the first idealization. However, it should be noted that spar flanges and stringers also serve as boundaries for the skin and web panels in each bay. In the local buckling calculations, the boundaries of the skin and web panels are assumed to be simply supported. To provide real simple support boundary conditions, the spar flange and stringer dimensions must be of certain size. Therefore, in practice the actual spar flange and stringer areas may have to be increased to provide the required boundary conditions for the skin and the web panels. However, since this study specifically deals with the preliminary design stage, the details of the spar flange and stringer areas are not considered in design process.

Figures 11 and 12 show the variation of the spar cap and stiffener areas along the wing span for both structural idealizations. Figures 11 and 12 give the results of the design performed based on the external loading calculated at point A on the V-N diagram. As shown in Figs. 11 and 12, in the first idealization spar and stiffener areas become decrease towards the wing tip because in the first idealization bending loads are carried by the spars and stringers. However, in case of second idealization, second smallest area from the standard area list is found to be sufficient to prevent overstressing of the spar flange or the stringer on the upper skin. The overall inertia of the wing section, supported by the inertia of thin walled panels, becomes sufficiently high that small spar cap areas are enough for the structural integrity of the spar caps or the stringers. Obviously, from a practical point of view such small spar cap or stringer areas may not be acceptable. However, as long as practical constraints are included in the design process, the simplified method of analyses which are summarized in this article can be transformed into more robust but simplified analysis tools based on simple beam theory.

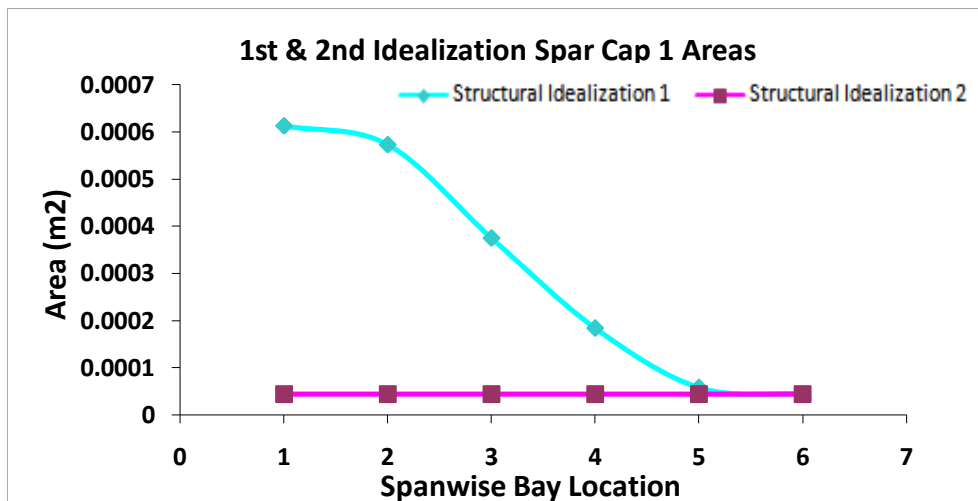


Figure 11. Spanwise variation of the area of the upper flange of the front spar

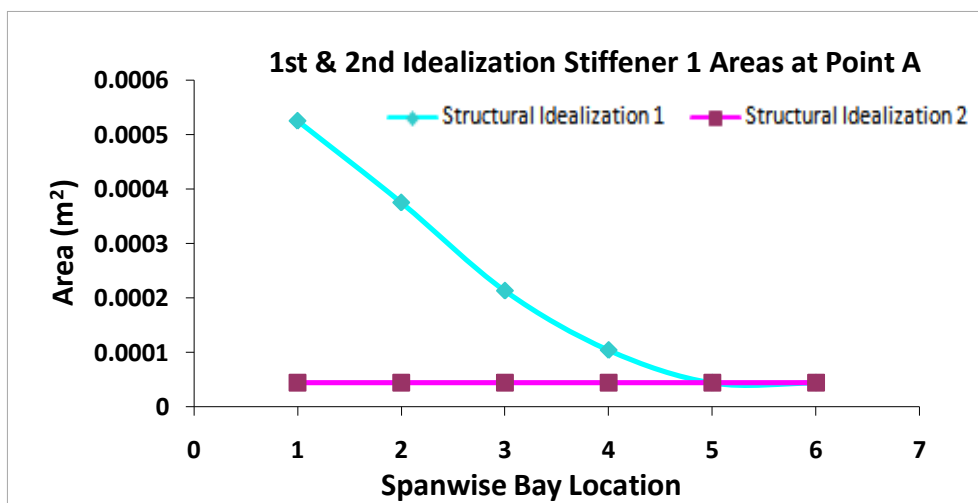


Figure 12. Spanwise variation of the area of the stringer on the upper skin

In the first structural idealization, the skin and spar web thicknesses are first determined such that they can carry the maximum shear stresses acting on them safely and then the buckling constraints are checked. Finally, the thicknesses are selected to safely satisfy both shear strength and buckling constraints. In the second idealization, since skins and spar webs also carry axial load, maximum Von-Mises stresses are calculated in each bay and strength check is first made based on the maximum Von-Mises stress acting at the inboard edge of each bay. Then, buckling check of each panel between the ribs stations are carried out. Thus, sizing is based on two level check of strength and satisfaction of the buckling constraints. Figures 13 and 14 show the nose skin and the front spar web thickness variations along the span of the wing for the first and second structural idealizations based on the loading calculated at the minimum maneuvering speed and maximum positive load factor.

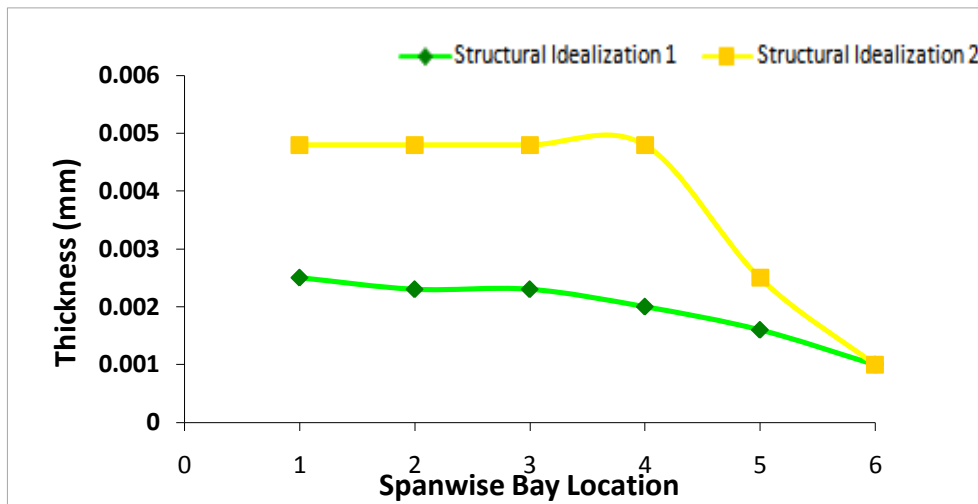


Figure 13. Spanwise variation of the nose skin thickness for the 1<sup>st</sup> and the 2<sup>nd</sup> structural idealization

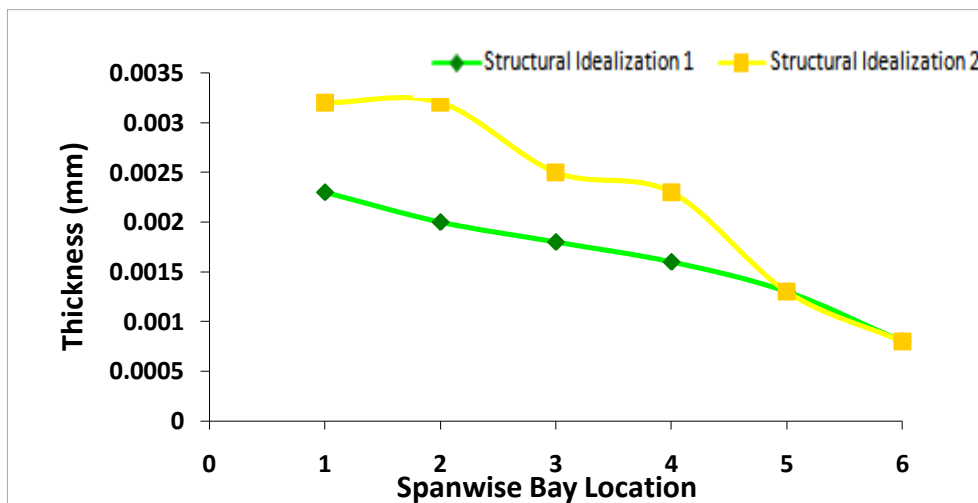


Figure 14. Spanwise variation of the front spar web skin thickness for the 1<sup>st</sup> and the 2<sup>nd</sup> structural idealization

As shown in Figures 13 and 14, in the second idealization nose skin and front spar web thicknesses are generally higher compared to the corresponding thicknesses determined based on the first structural idealization. The trend in the thickness variation is in accordance with the mass breakdown bar chart given in Fig. 10. However, not all the skin panels follow the same trend. For instance, as Fig. 15 shows, in bays away from the wing root structural idealization 1 predicts higher skin thickness. It should be noted that skins thicknesses are determined as a result of two level checks of strength and

local buckling. In general, it is experienced that local buckling condition is the main driver of the design. In the first structural idealization shear stress ratio given by Eq. (1) is used for the local buckling check. For the second structural idealization, the interaction equation given by Eq. (2) is used for the local buckling check for the upper skin panels which are under combined shear and compression. If local buckling drives the design, then shear stress ratio ( $R_s$ ) and the compression stress ratio ( $R_c$ ) are the critical factors which determine the final thicknesses of the upper skin panels. It should be noted in the interaction equation given by Eq. (2), shear stress ratio is squared, whereas in the first structural idealization, shear stress ratio is used in the local buckling check. Therefore, to decide on which structural idealization gives higher thickness for the upper skin panels, relative magnitudes of the shear stresses predicted by the first and second structural idealizations and the compression stress ratio have to be checked. Based on the thickness plot given in Fig.15, it can be said that after bay 2, the left hand side of Eq. (2) becomes smaller than the shear stress ratio Eq.(1) which is determined for the first structural idealization.

$$R_s = \left( \frac{\tau}{K_s E \left( \frac{t}{b} \right)^2} \right) \leq 1 \tag{1}$$

$$R_s^2 + R_c \leq 1 \tag{2}$$

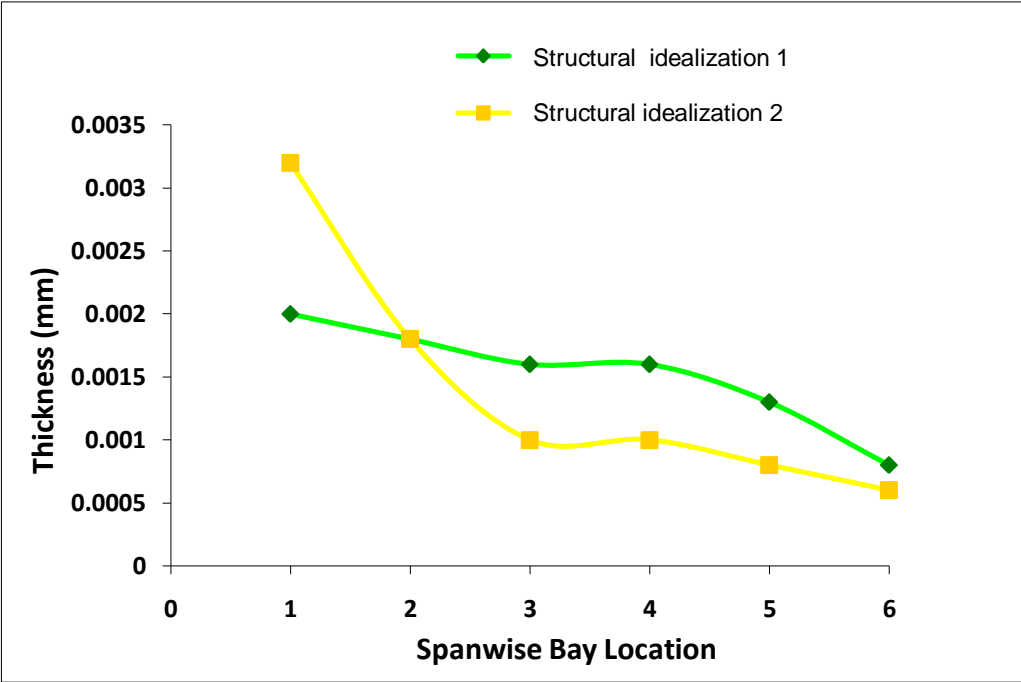
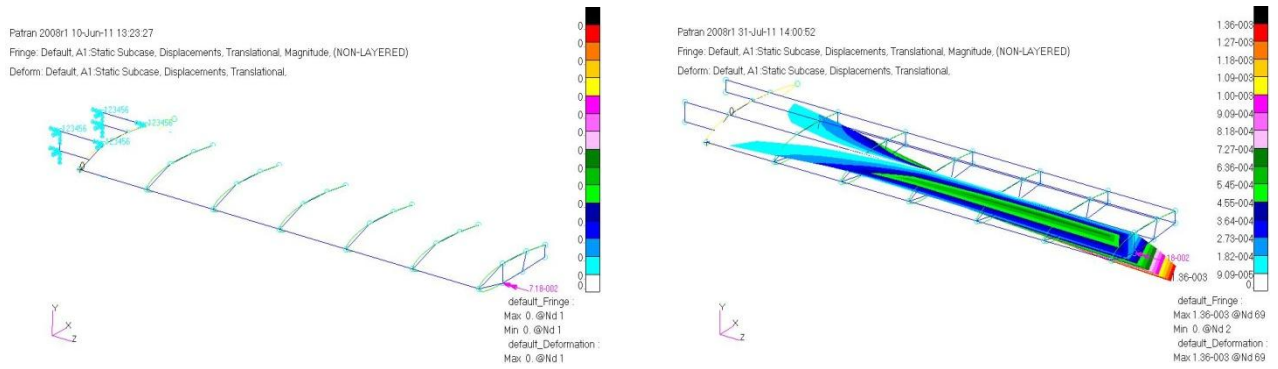


Figure 15. Spanwise variation of the upper middle skin thickness for the 1<sup>st</sup> and the 2<sup>nd</sup> structural idealization

**Finite element analysis of the wing structure using different one and two dimensional element combinations**

This section introduces the finite element models of the wing structure which are generated by using different one and two dimensional element pairs. The main objective of finite element analysis study is to investigate the effect of using different finite element types on the analysis results of the wing torque box, which is designed by the simplified method using structural idealizations, and also to make comparisons between the analysis results of finite element solution and the results obtained by the

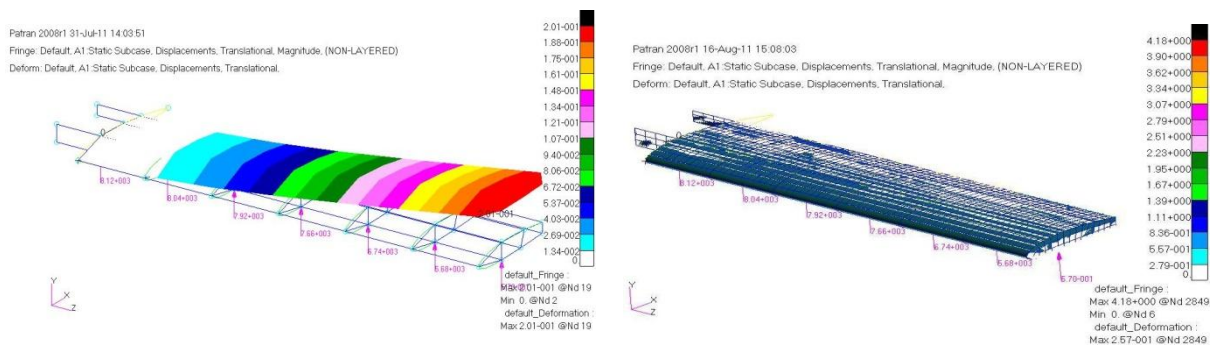




(a) Membrane elements without drilling dof (b) Membrane elements with drilling dof

Figure 17. Deformation plots under pure distributed pitching moment

Another simple case study of the wing under distributed lift loading shows that for the fine mesh case, the deformation shape of the wing modeled with revised formulation membrane elements in the finite element model does not reflect the true deformation. Figure 18 shows the deformation plots of the wing structure, for the coarsest and finest mesh, under distributed lift loading acting through the lower flange of the front spar. Figure 18 confirms that membrane elements with drilling degrees of freedom must be used with the coarsest mesh in order for the wing to respond to distributed lift loading and predict the deformation accurately. It should be noted that since the middle elements in the chord direction does not deform in the out of plane direction, fine mesh finite element model does not predict the true deformation shape of the wing even though membrane elements with drilling degrees of freedom are used on the wing ribs. In addition, it is also noticed that although the distributed lift loading is acting through the front spar, there is very little twisting of the wing structure. Little twisting of the wing is attributed to the presence of ribs in the wing which provide additional torsional stiffness.



(a) Membrane - R elements with coarsest mesh (b) Membrane - R elements with Finest Mesh

Figure 18. Deformation plots under distributed lift force

Based on the sample examples presented, it is concluded that in order to handle the distributed pitching moment and distributed lift loading accurately, revised formulation membrane elements must be used on the wing ribs. In addition, single elements must be used between the rib stations, and also in chord-wise direction between the spars and stringers.

Before performing the finite element analysis of the wing structure models, it is important to guarantee that the model contains a sufficient number of elements in order to arrive at the correct solution. Therefore, mesh size study has to be performed to make sure that converged solutions are obtained. In the current study, the coarsest mesh corresponds to the use of single elements between the rib stations. To investigate the effect of the mesh size on the displacement and stress results, the wing structure is modeled with three different mesh sizes. The first model is the coarsest mesh model that is generated by using a single element between the ribs. In the coarsest mesh, total number of one

dimensional and two dimensional elements is 107. The second model is a fine mesh model which is less coarser than the first model and the total number of one dimensional and two dimensional elements is 819. The last model is the finest mesh model, and it contains a total number of 3097 of one dimensional and two dimensional elements. Figure 19 shows the three different mesh sizes used in the convergence study. Mesh convergence study is performed for all pairs of elements listed in Table 2. In the convergence study, tip displacement and Von Mises stress results of the wing are used as the parameters to monitor the effect of using different mesh sizes and to ensure that a converged solution is achieved. Table 3 summarizes the maximum tip displacement and the Von Mises stresses obtained at the center of the middle upper skin (Fig.1) of bay 4 (Fig.8) for rod/shell model with three mesh densities. Results in Table 3 shows converged solutions are achieved in terms of tip displacement and Von-Mises stresses. As expected, even with the coarse mesh, converged solution is reached. However, in terms of stresses finer mesh is needed for convergence. In the current study, the results of the coarse mesh and the finest mesh finite element models are used to make comparative study with the results of the simplified method of analysis using structural idealizations 1 and 2.

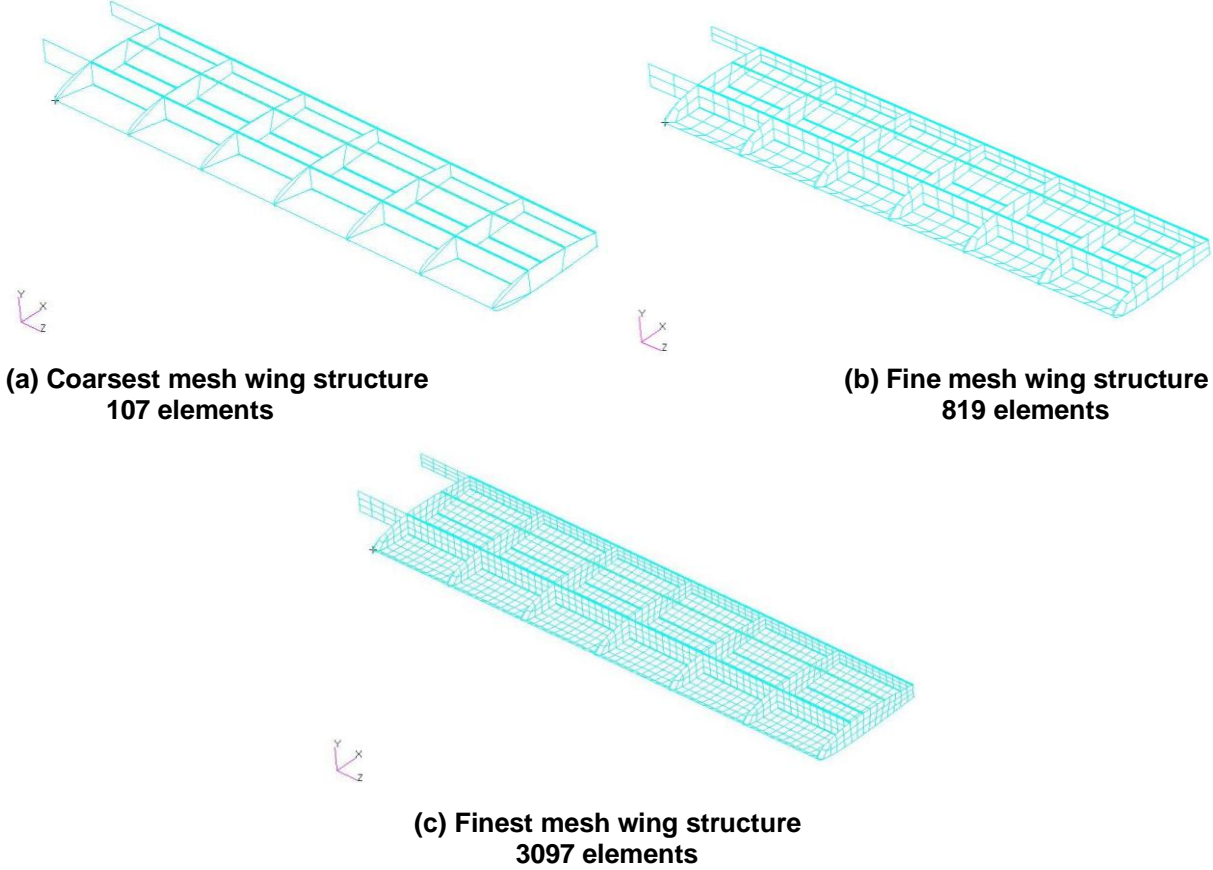


Figure 19. Finite element models of the wing structure with three different mesh sizes

Table 3. Comparison of the maximum tip displacement and the Von Mises stresses

Mesh Density	Tip Displacement (cm)	Von – Mises Stress (MPa)
Coarsest – 107 elements	18.5	40.35
Fine – 819 elements	17.5	24.37
Finest – 3097 elements	18.4	25.83

## Comparison of the Von Misses stresses determined by FEA method and the simplified method of analysis

The finite element analysis of the wing structure for the coarse mesh case is performed for all models given in Table 2 and comparisons are made. On the other hand, for the fine mesh case, finite element solutions are not performed for the models which have revised membrane elements. For the different finite element models listed in Table 2, Von Misses stresses calculated at the centers of bays 2-5 on the upper middle skin (Fig.1) are compared in Tables 4 and 5 for the coarsest and the finest mesh finite element models, respectively. Tables 4 and 5 also show the Von Misses stresses determined by the simplified method using the structural idealization 2 at the same locations on the upper skin. In Tables 4 and 5, bays 1 and 6 are not included, because these bays are at the boundaries of the wing, and stresses determined by the simplified method of analysis are not affected by the presence of the boundaries. Therefore, to make more reliable comparison of the stresses determined by the finite element models and the simplified method of analysis, Von Misses stresses in bays 2-5 are compared.

**Table 4. Von-Misses stresses at the center of the middle upper skin-Coarsest Mesh**

Model	Von Misses Stresses (MPa)			
	Bay 2	Bay 3	Bay 4	Bay 5
Rod/Shell	125.50	77.89	40.35	18.49
Beam/Shell	124.06	75.28	37.78	16.42
Rod/Shell-R	125.64	76.70	39.31	18.45
Beam/Shell-R	127.23	76.08	38.15	16.34
Rod/Membrane-R	133.05	77.11	38.66	17.26
Beam/Membrane-R	131.42	75.33	36.88	15.08
Simplified Method <sup>1</sup>	106.82	75.70	39.80	22.19

<sup>1</sup> Structural idealization 2

**Table 5. Von-Misses stresses at the center of the middle upper skin-Finest Mesh**

Model	Von Misses Stresses (MPa)			
	Bay 2	Bay 3	Bay 4	Bay 5
Rod/Shell	81.40	57.95	25.83	11.12
Beam/Shell	81.74	57.62	25.53	10.72
Rod/Shell-R	80.66	57.34	25.64	11.02
Beam/Shell-R	81.03	57.07	25.28	10.50
Simplified Method <sup>2</sup>	106.82	75.70	39.80	22.19

<sup>2</sup> Structural idealization 2

Tables 4 and 5 show that Von Misses stresses calculated by the fine mesh finite element models are actually lower than the Von Misses stresses calculated by the coarse mesh models at the identical locations on the wing structure. Tables 4 and 5 also show that there are no drastic differences in the Von Misses stresses predicted by the shell models with rod or beam flanges. For both coarse and fine mesh cases, it is seen that in general Von Misses stresses predicted by the finite element models with beam elements are slightly lower than the Von Misses stresses predicted by the finite element models with rod elements. Such a difference could be expected because beam elements have higher degrees of freedom than the rod elements, and therefore wing structure modeled with beam elements is slightly more flexible which might have resulted in slight stress relaxation. However, especially for the fine mesh models the difference is negligible. At this point, it should be noted that in the finite element models, for the rod element only axial stiffness is considered. Thus, rod element essentially behaves like the one dimensional reinforcing members used in the simplified method of analysis. On the other hand, in the finite element models, beam cross sections are taken as thin rectangular cross-sections representing the spar and the stringer caps.

It is also observed from Tables 4 and 5 that the use shell elements with drilling degrees of freedom does not have a major effect on the Von Misses stresses obtained by the coarse and the fine mesh finite element models away from any structural discontinuity. The standard shell elements on the spar webs and on the lower skin take up the distributed lift and pitching moment load accurately.

Based on the comparison of the Von Misses stresses determined by the finite element solution and the simplified method of analysis using the second structural idealization given in Tables 4 and 5,

several conclusions can be drawn. It should be noted that finite element models are two dimensional models, whereas in the simplified method one dimensional beam model is used. Therefore, finite element models are more flexible compared to the beam model of the simplified method, and the strain energy distribution is two dimensional in the finite element models. Therefore, in general one can expect to have lower stresses in the finite element model away from any structural discontinuity. Fine mesh results given in Table 5 confirm that Von Misses stresses predicted by the simplified method are consistently higher than the Von Misses stresses predicted the by the fine mesh finite element models. One main effect which is not considered in the simplified beam model is the axial stresses generated in the flanges and skins due to torsion. The effect of neglecting the torsion effect on the axial stresses is clearly seen in Table 5, from the increasing ratio of the Von Misses stresses determined by the finite element solution to the Von Misses stresses calculated by the simplified method. On the other hand, Von Misses stresses determined by the coarse mesh finite element models and the simplified method are very close to each other in bays 3 and 4, which are away from the restraint end and the free edge boundary at the wing tip. The closeness of the Von Misses stresses in the mid bays is due to the fact that coarse mesh finite element models behave more stiff compared to fine mesh finite element models, and therefore beam model of the simplified method can be best simulated by the coarse mesh finite element models. Table 4 also shows that towards the wing root, coarse mesh finite element models predict higher stress than the simplified method. Combination of the boundary and the torsion effect on the axial stresses is considered to be the main reason for the higher Von Misses stresses predicted by the finite element models in the bay 2.

### Comparison of the axial stresses determined by FEA method and simplified method of analysis

For the different finite element models listed in Table 2, axial stresses calculated at the centers of bays 2-5 on the upper spar cap of the front spar (Fig.1) are compared in Tables 6 and 7 for the coarsest and finest mesh finite element models, respectively. Tables 6 and 7 also show the compressive axial stresses determined by the simplified method using the structural idealization 2 at the same locations.

**Table 6. Axial stresses on the upper spar cap of the front spar - Coarsest Mesh**

<b>Compressive Axial Stresses - (MPa)</b>				
<b>Model</b>	<b>Bay 2</b>	<b>Bay 3</b>	<b>Bay 4</b>	<b>Bay 5</b>
<b>Rod/Shell</b>	116.75	80.74	37.19	17.36
<b>Beam/Shell</b>	112.75	77.74	35.56	15.46
<b>Rod/Shell-R</b>	117.43	80.73	37.60	17.97
<b>Beam/Shell-R</b>	115.94	79.11	36.12	15.79
<b>Rod/Membrane-R</b>	118.21	80.52	37.13	17.85
<b>Beam/Membrane-R</b>	116.56	78.76	35.56	15.52
<b>Simplified Method<sup>3</sup></b>	114.60	80.00	41.70	19.30

<sup>3</sup> Structural idealization 2

**Table 7. Axial stresses on the upper spar cap of the front spar - Finest Mesh**

<b>Compressive Axial Stresses - (MPa)</b>				
<b>Model</b>	<b>Bay 2</b>	<b>Bay 3</b>	<b>Bay 4</b>	<b>Bay 5</b>
<b>Rod/Shell</b>	80.96	51.96	21.60	8.07
<b>Beam/Shell</b>	80.84	51.95	21.70	8.12
<b>Rod/Shell-R</b>	80.40	51.22	21.53	7.93
<b>Beam/Shell-R</b>	80.29	51.25	21.48	8.03
<b>Simplified Method<sup>4</sup></b>	114.60	80.00	41.70	19.30

<sup>4</sup> Structural idealization 2

As mentioned previously, In Tables 3 and 4, bays 1 and 6 are not included, because these bays are at the boundaries of the wing, and stresses determined by the simplified method of analysis are not affected by the presence of the boundaries. Therefore, to make more reliable comparison of the axial stresses determined by the finite element models and the simplified method of analysis, axial stresses in bays 2-5 are compared.

Tables 6 and 7 show that similar to the Von Misses stresses, axial stresses calculated by the fine mesh finite element models are lower than the axial stresses calculated by the coarse mesh models at the identical locations on the wing structure. Tables 6 and 7 also show that there are no drastic

differences in the axial stresses predicted by the shell models with flanges and stringers modeled with rod or beam elements. For both coarse and fine mesh cases, it is seen that in general axial stresses predicted by the finite element models with beam elements are slightly lower than the axial stresses predicted by the finite element models with rod elements. Such a difference could be expected because beam elements have higher degrees of freedom than the rod elements, and therefore wing structure modeled with beam elements is slightly more flexible which might have resulted in slight stress relaxation. However, especially for the fine mesh models the difference is negligible.

Similar to the situation for the Von Misses stress case, axial stresses determined by the simplified method of analysis in bays 2-5 are consistently less than the axial stresses determined by the fine mesh finite element models. It should again be noted that in the simplified beam model, axial stresses generated in the spar flanges and stringers due to torsion are not considered because of the free warping assumption. For both coarse and fine mesh finite element models, the effect of neglecting the torsion effect on the axial stresses is clearly seen in Tables 6 and 7, from the increasing ratio of the axial stresses determined by the finite element solution to the axial stresses calculated by the simplified method towards the inboard bays.

Results given in Table 6 show that axial stresses predicted by the simplified method and the coarse mesh finite element models are very close to each other in bays 2-5. Since the coarse mesh finite element models behave more stiff compared to fine mesh finite element models, it can be concluded that simplified method based on unsymmetric beam theory can be best simulated by the coarse mesh finite element models. Or, one can comment that instead of coarse mesh finite element models, one can use the simplified method of analysis in the preliminary design stage with confidence.

It is also observed from Tables 6 and 7 that the use shell elements with drilling degrees of freedom does not have a major effect on the axial stresses obtained by the coarse and the fine mesh finite element models. The standard shell elements on the spar webs and on the lower skin take up the distributed lift and pitching moment load accurately. Based on the results for the Von Misses and axial stresses, it can be concluded that the use of standard shell elements without drilling degrees of freedom in modeling the semi-monocoque wing structures is justified. There is no major advantage in using shell elements with drilling degrees of freedom in the finite element models of semi-monocoque wing structures.

**Comparison of maximum Von Misses stresses determined by the fine and coarse mesh finite element models**

In this section, maximum Von Misses stresses determined by the fine and coarse mesh finite element models listed in Table 2, are compared with each other. Figures 20 and 21 show the Von Misses stress distribution for the rod/shell model for the coarsest and the finest mesh FE models.

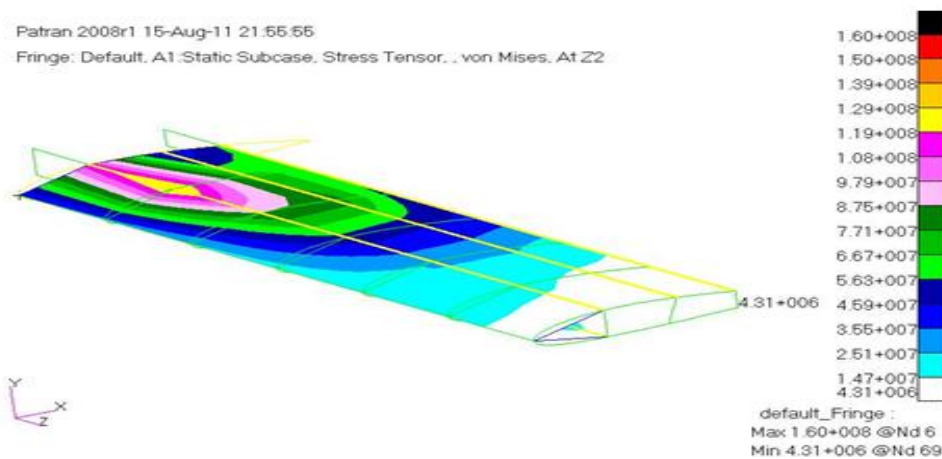


**Figure 20. Von Misses stress distribution– Coarse mesh Rod/Shell model**

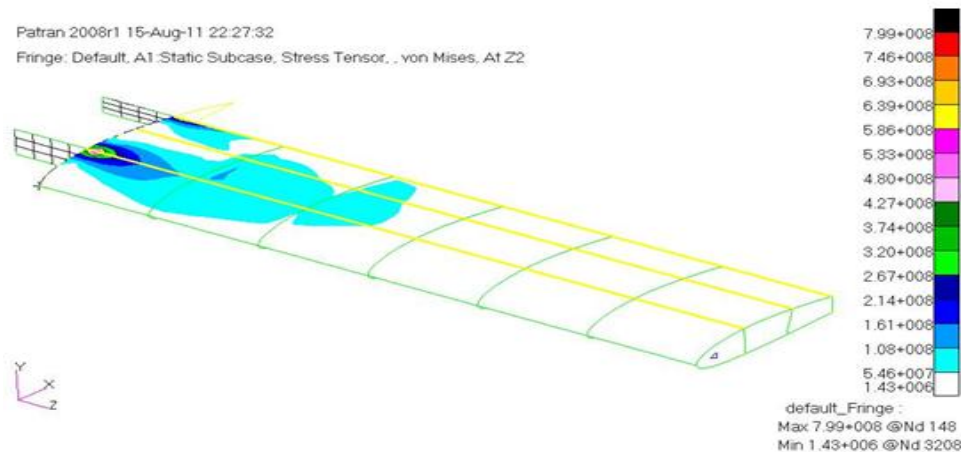


**Figure 21. Von Mises stress distribution– Fine mesh Rod/Shell model**

Von Mises stress plots of the finest mesh case clearly show that the peak stresses occur at the front spar wing root intersection in a very confined area. From color scales in Figs. 20 and 21, it can be seen that the maximum stress of the fine mesh rod/shell model is much higher than the maximum stress of the coarse mesh rod/shell finite element model. Table 8 gives the maximum Von Mises stresses determined by the finest and coarsest mesh for the different finite element models listed in Table 2. For the finest mesh case, membrane elements are excluded from the comparison, because of the deficiency of finest mesh membrane model in handling the distributed line force and pitching moment loading accurately.

**Table 8. Comparison of maximum Von Mises stresses (Mpa)**

Maximum Von – Mises Stress (MPa)		
Model	Coarsest Mesh	Finest Mesh
Rod/Shell	160	799
Beam/Shell	151	797
Rod/Shell-R	149	738
Beam/Shell-R	148	737
Rod/Membrane-R	147	----
Beam/Membrane-R	146	----

Figures 20 and 21 and Table 8 show that for all the finite element models, maximum Von Mises stresses determined by the finest mesh models are higher than the maximum Von Mises stresses determined by the coarsest mesh models. It should be noted that although the Von Mises stresses calculated by the fine mesh finite element models are lower than the Von Mises stresses calculated by the coarse mesh models at the identical locations on the wing structure away from any structural discontinuity, such as at the center of bays 2-5 on the upper middle skin, since the fine mesh finite element models capture the stress gradients better, the maximum stresses predicted by the fine mesh models are higher than the maximum stresses predicted by the coarse mesh models.

Table 8 also shows that the maximum Von Mises stresses determined by the finite element models with the standard shell elements are slightly higher than the maximum Von Mises stresses determined by the finite element models with the shell elements with drilling degrees of freedom. Maximum Von Mises stresses near the the front spar wing root intersection reduces when shell elements with drilling degrees of freedom are used in the finite element model. Normally, a finite element model with shell elements having drilling degrees of freedom is more flexible compared to the finite element model with standard shell elements. Therefore, the reduction of the maximum Von Mises stress in finite element models with shell elements having drilling degrees of freedom is attributed to the additional flexibility introduced through the inclusion drilling degrees of freedom.

It is should be noted that maximum Von Mises stresses in linear finite element analysis continue to increase beyond the yield stress as the mesh size decreases. Von Mises stress plots of the finest mesh case clearly show that the peak stresses occur at the front spar wing root intersection in a very confined area. Spar root is a singular point because in the finite element analyses, all the rotations and displacements of the nodes on the wing root extensions are fixed, and this is a very stringent

condition. Because in reality a perfect fixed end condition is hard to achieve, and therefore maximum Von Mises stresses near the front spar-wing root will be relaxed. Therefore, it would not be logical to continue commenting on the reasons of the peak Von Mises stress near the front spar-wing root intersection without generating a local model of the wing root and carrying out a finite element analysis on the local model. Such a local analysis would give more realistic stresses and would give more insight into the actual behavior of the wing structure near the intersection of the front spar and the wing root.

## CONCLUSION

In the present article, a comprehensive study on the effect of using different structural idealizations on the design and analysis of thin walled semi-monocoque wing structures in the preliminary design phase is performed. The wing structures are designed using two different structural idealizations that are typically used in the preliminary design phase, and the finite element analysis of one of the designed wing configurations is performed using six different one and two dimensional element pairs which are typically used to model the sub-elements of semi-monocoque wing structures. The effect of using different finite element types on the analysis results of the wing structure, which is designed by the simplified method using two different idealization approaches, is investigated. Comparisons are also made between the analysis results of the finite element solution and the simplified method, and the applicability of the simplified method in the preliminary design phase is investigated for the wing configuration studied in the article. During the analysis study, depending on the mesh size used, conclusions are also inferred with regard to the deficiency of certain element types in handling the true external load acting on the wing structure.

Designs performed using the first and the second structural idealizations showed that the use of second structural idealization results in approximately 10 kg lighter mass in the final configuration compared to the use of first idealization during the design analysis. It is concluded that the mass of the spar flanges and the stringers account for the higher mass of the final configuration wing structure, which is designed using the first structural idealization.

Finite element analyses of the wing structure with different element types showed that the distributed line lift and pitching moment loading, which is used as the external load in the current study, necessitates the use of revised membrane elements in the wing ribs, because with the standard membrane elements in the wing ribs, the distributed pitching moment cannot be handled accurately. It is also concluded that in order to handle the distributed pitching moment accurately, single elements must be used between the rib stations in the finite element models with revised membrane elements. Finite element analyses of the wing structure with different element types showed that away from any structural discontinuity, stresses predicted by the fine mesh finite element models are less than the stresses predicted by the coarse mesh finite element models at the identical locations on the wing structure. However, since fine mesh finite element models capture the stress gradients better, the maximum stresses predicted by the fine mesh models are usually higher than the maximum stresses predicted by the coarse mesh models.

In general, stresses predicted by the finite element models with beam elements are slightly lower than the stresses predicted by the finite element models with rod elements. Flexibility introduced by the beam elements is considered to be the main reason for the slightly lower stresses predicted by the finite element models which have flanges and stringers modeled with beam elements compared to the finite element models which have flanges and stringers modeled with rod elements.

Maximum Von Mises stresses determined by the finite element models with the standard shell elements are slightly higher than the maximum Von Mises stresses determined by the finite element models with the shell elements with drilling degrees of freedom. The reduction of the maximum Von Mises stress in finite element models with shell elements having drilling degrees of freedom is attributed to the additional flexibility introduced through the inclusion of drilling degrees of freedom. However, the use shell elements with drilling degrees of freedom does not have a major effect on the stresses obtained by the coarse and the fine mesh finite element models away from any structural discontinuity. Von Mises stresses determined at the centers of the upper middle skin in bays 2-5, and the axial stresses determined at the centers of the upper flange of the front spar in bays 2-5 confirm this conclusion.

Finite element analyses by the fine mesh finite element models showed that stresses predicted by the simplified method, using the second structural idealization, are consistently higher than the stresses predicted by the fine mesh finite element models. On the other hand, stresses determined by the coarse mesh finite element models and the simplified method agree with each other closely in most of

the bays which are away from the restraint end and the free edge boundary at the wing tip. Since the coarse mesh finite element models behave more stiff compared to fine mesh finite element models, it is concluded that simplified method based on unsymmetric beam theory can be best simulated by the coarse mesh finite element models. It is also observed that axial stresses determined by the coarse mesh finite element models and the simplified method of analysis agree better than the Von Misses stresses.

Based on the results presented in the article, it is concluded that with the simplified methods, preliminary sizing of the wing structures can be performed with enough confidence. Results of the simplified method of analysis showed that simplified method is applicable to be used as an analysis tool in performing the preliminary sizing of the wing structure before moving on to more refined finite element based analysis.

## REFERENCES

- [1] Aircraft Spruce and Specialty Co., <http://www.aircraftspruce.com>, last accessed date on 10<sup>th</sup> January 2011
- [2] Schaeffer, H.G., *MSC.Nastran Primer for Linear Static Analysis*, MSC Software Corporation, Santa Ana, California 2001.
- [3] FAA Federal Aviation Regulations (FARS, CFR 14), FARS PART 23 Appendix A, A.23.1 General, [http://www.flightsimaviation.com/data/FARS/part\\_23-appA.html](http://www.flightsimaviation.com/data/FARS/part_23-appA.html) , last accessed date on 23<sup>rd</sup> April 2009
- [4] Howe, D., *Aircraft Loading and Structural Layout*, AIAA Publication, VA, USA, 2004.
- [5] Vaughan, R.E., Daniel M.F., *The Correct use of Finite Element Models for Stress Analysis of Aircraft*, Annual Forum Proceedings, Vol. 60, Part 1, pp. 140-192, American Helicopter Society, 2004.
- [6] Niu, Michael C.Y., *Airframe Structural Design*, Second edition, Hong Kong Conmilit Press Ltd., Hong Kong,1999.
- [7] MIL-HDBK-5H: Military Handbook Metallic Materials and Elements for Aerospace Vehicle Structures, Department of Defense, USA, December 1998
- [8] Niu, Michael C.Y., *Airframe Stress Analysis and Sizing*, Second edition, Hong Kong Conmilit Press Ltd., Hong Kong,1997.
- [9] ESDU 95010, *Computer program for estimation of span-wise loading of wings with camber and twist in subsonic attached flow*, <http://www.esdu.com>, June 1995.
- [10] Megson, T.H.G., *Aircraft Structures for Engineering Students*, Second edition, John Wiley and Sons, New York, USA, 1990.
- [11] Bruhn, E.F., *Analysis and Design of Flight Vehicle Structures*, Tri-State Offset Company, USA, 1973.
- [12] Peery, D.J., *Aircraft Structures*, McGraw Hill, First Edition, New York, USA, 1950.